Prediction of fiber rotation in an orifice channel during injection molding process

Tu Thien Ngo,[1,2,3] Hoang Minh Khoa Nguyen,[1] and Dong-Wook Oh[1,a)]

[1]*Department of Mechanical Engineering, Chosun University, Gwangju 61452, South Korea*
[2]*Faculty of Mechanical Engineering, Ho Chi Minh University of Technology (HCMUT), 268 Ly Thuong Kiet Street, District 10, Ho Chi Minh City, Vietnam*
[3]*Vietnam National University Ho Chi Minh City, Linh Trung Ward, Thu Duc District, Ho Chi Minh City, Vietnam*

(Received 10 June 2021; final revision received 27 September 2021; published 14 October 2021)

Abstract

Additive alignment in polymer composites can enhance the physical properties of the constitutive material. Researchers have attempted to understand and predict the additive orientation during the fabrication process, such as injection molding. In this study, the rotation of carbon fibers embedded in uncured polydimethylsiloxane flowing in an orifice channel is analyzed via a flow visualization experiment and image processing of obtained images. The angular velocity of additives is correlated with the shear rates in the flow field calculated from the computational fluid dynamics simulation with the assumption of a single-phase and a non-Newtonian flow. The effective shear rate is found to have a larger effect on the rotation of fiber compared with the aspect ratio of the fiber and the initial alignment angle to the flow direction. A correlation between the effective shear rate and angular velocity of the fibers is developed and verified experimentally. This correlation can be used to predict the fiber rotation during polymer composite fabrication within an orifice channel and hence provide useful information regarding the anisotropic physical properties of the final product. https://doi.org/10.1122/8.0000314

I. INTRODUCTION

Additive alignment in a viscous fluid during the injection molding of composite materials is an essential topic in material science and engineering. This is because the physical properties of polymer composites are significantly affected by the additive fiber alignment inside the mold channels during the fabrication process [1–4]. Additionally, additive alignment along the direction of the molten polymer flow results in the final product having anisotropic physical properties. Over the last century, Jeffery [5] proposed a comprehensive theoretical model to describe the motion of an ellipsoidal particle immersed in a viscous fluid under a simple shear flow. Some works were performed to analyze and verify Jeffery's model through experimental and theoretical studies [6,7]. In addition, researchers have developed sophisticated models to describe the alignment and orientation of fiber-type additives in suspension. Theories and models that describe additive rheology in probability distribution functions and orientation tensor components have been reported [8–11]. These models were utilized in computational fluid dynamics (CFD) simulations to predict the effective alignment of fibers during the fabrication of polymer composites [12–17].

The configuration of the mold channel is one of the major parameters that affect the orientation of fibers during the manufacturing process of polymer composites. Studies have been conducted to experimentally analyze additive alignments in various shaped channels, such as a parallel plate channel, an abrupt contraction channel [18], and a channel containing a cylindrical block [19]. To observe fiber alignment in a mold channel flow, an image processing method was developed to track a rapid angle change of fibers flowing with a liquid polymer base [20]. The proposed technique was applied to compute the angle, length, and location of fibers passing through an orifice channel that resembled the gate of an injection mold. The results from the flow visualization of additives were compared with the velocity flow field from CFD calculations to facilitate the understanding of the rheology of additives [21–23]. Trebbin *et al.* [24] investigated the perpendicular alignment of fiber-type additives passing through a convergence and divergence channel. A flow visualization experiment was performed by using x-ray scattering technique to quantitatively measure the alignment angles of the additives inside the channel. The alignment angles were mapped with the different components of flow shear rates calculated via CFD simulation with the assumption of a single-phase and a non-Newtonian fluid flow. The ratio of the extension rate (a perpendicular gradient component of a perpendicular directional velocity to the flow direction) to the shear rate (a parallel gradient component of a parallel directional velocity to the flow direction) was calculated to describe the fiber orientation in the microchannels with Newtonian and non-Newtonian fluids. They discovered that a ratio exceeding 0.14 represented a perpendicular alignment of fibers inside a divergence channel. However, in their study, the ratio value can be used to only assess whether an overall perpendicular or parallel alignment was present inside the channel and the quantitative analysis of the alignment angle was not possible by using such a ratio.

Such observation and analysis of individual fibers flowing inside a flow channel are considered to be very important in understanding the rheology of additives. Data of additive

a)Author to whom correspondence should be addressed; electronic mail: dwoh@chosun.ac.kr

angle, rotation, and movement can be correlated with the location in the channel, channel configuration, velocity field, shear rates, etc., to constitute a general correlation of additive alignment inside a mold. This approach may be considered as a "bottom-up" approach in comparison to the "top-down" approach of conventional theories and models [25–30] where the governing equation of the flow and additive orientation need to be solved to calculate the additive alignment angle. To predict the orientation angle of the fiber inside a mold channel, shear and extension rates of the flow field need to be correlated to the rotation of the fiber. Just like in Jefferey's equation, the rotational velocity of an ellipsoid is a function of the aspect ratio of fiber, initial angle, and shear rate [5]. The orientation angle of fibers can be calculated after the integration of calculated rotational velocity along the fiber movement trajectory.

In this article, to develop a more detailed and simpler index that can quantitatively describe the rotation of fiber in a mold channel, the flow visualization of milled-carbon fiber and uncured polydimethylsiloxane (PDMS) mixture was performed. The movement and rotation of fibers inside an orifice channel that mimic the gate of an injection mold channel were analyzed. Changes in the location, velocity, angle, and angular velocity of fiber were calculated from image processing of sequential images obtained from flow visualization. A separate CFD calculation of an identical configuration of the orifice channel was performed to calculate the shear and extension rates exerted on the fiber. Moreover, a correlation of the angular velocity as a function of the shear and extension rates was developed and validated by comparing it to the experiment data. We believe the obtained correlation is more simple, straightforward and requires less computational power to calculate the alignment angle of additives in an orifice channel compared to conventional models and methods. Additionally, the approach should enhance our understanding of additive alignment during the molding process and can be used to validate and enhance the accuracy of conventional models.

II. MODELING AND NUMERICAL SIMULATION

The movement behavior of a fiber flowing in a flow field is affected by many factors. The most significant factor is the shear stress exerted on the additive due to the surrounding flow field. The movement and rotation of a fiber can be determined if all the shear stresses on the fiber were to be identified and summed. In this study, a diluted fiber suspension where fiber–fiber and fiber–wall interactions are negligible was considered. The movement and rotation of a fiber were assumed to be induced by the flow only. The behavior of the fiber inside a flow is shown in Fig. 1. The angle (θ) of the fiber with respect to the direction of the flow was assumed to change from θ_1 to θ_2. The angle of a fiber is defined in a counter-clockwise direction based on the 3 o′clock direction. The shear stresses on a fiber can be categorized into gradients of x- and y-velocity components corresponding to u and v, respectively. As shown in Fig. 1, the components of the shear rate $\dot{\gamma}(\partial u/\partial y)$ and extension rate $\dot{\varepsilon}(\partial v/\partial y)$ can be described by the deformation of a fluid lump exerted in a shear flow.

According to Jeffery [5], the motion of an ellipsoidal particle immersed in a simple shear flow can be expressed as the following equation:

$$\dot{\theta} = \frac{\dot{\chi}}{AR^2 + 1}(AR^2 \sin^2\theta + \cos^2\theta), \tag{1}$$

where $\dot{\chi}$, θ, and $\dot{\theta}$ are the effective shear rate, particle angle, and angular velocity, respectively. AR is the aspect ratio of the particle, defined as the length-to-diameter ratio. An effective shear rate can be defined as the following function of the shear and extension rates if the flow can be assumed

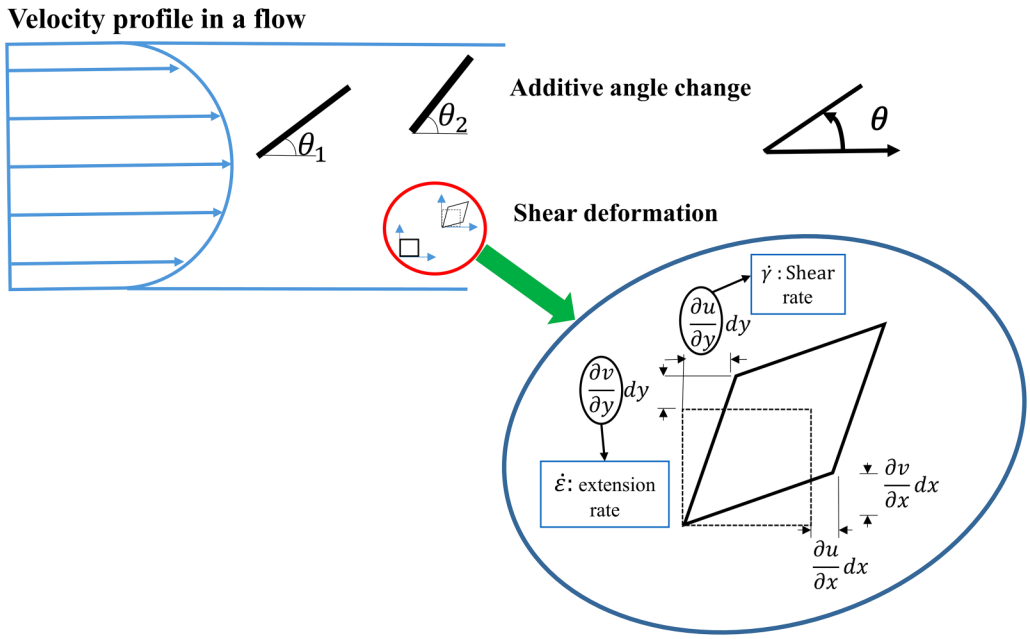

FIG. 1. Deformation and angle change of a flow lump and a fiber in the fluid flow.

as two-dimensional (2D) [31]:

$$\dot{\chi} = \sqrt{\frac{1}{2}\left|\frac{\partial u}{\partial y} \times \frac{\partial v}{\partial y}\right|}. \tag{2}$$

Based on Eq. (1), the angular velocity of an ellipsoid is a linear function of the effective shear rate and also a function of the initial angle with respect to the flow direction. The maximum and minimum angular velocities can be predicted at the initial angles of 90° or −90° and 0°, respectively.

An orifice channel, which resembles the gate channel of an injection mold, comprises a narrow channel connected to a sudden expansion channel, as shown in Fig. 2. To apply Jeffrey's model to a fiber passing a gate and traveling inside an injection mold, we can consider a trajectory of a fiber, as shown in Fig. 2. The fiber moved from position 1 with angle θ_1 to position 2 with angle θ_2. A local coordinate of the horizontal axis on the fiber trajectory can be defined to calculate the fiber angle with respect to the flow direction. The alignment angle of the fiber with respect to the flow direction can be defined as θ^* as in the following equation:

$$\theta^* = \overline{\theta} + \phi, \tag{3}$$

where ϕ is defined as the angle between the fiber trajectory and x axis and $\bar{\theta}$ is the average angle of θ_1 and θ_2. When comparing the trajectory and rotation of a fiber obtained from a flow visualization experiment to the theoretical calculation of Jefferey's model, θ^* must be calculated and used as an input value in Eq. (1). Then Eq. (1) becomes as follows:

$$\dot{\theta}^* = \frac{\dot{\chi}}{AR^2 + 1}(AR^2 \sin^2\theta^* + \cos^2\theta^*). \tag{4}$$

On the other hand, an angular velocity can be calculated from two consecutive images from a flow visualization experiment where alignment angles of a fiber with respective to the flow direction are θ_1^* and θ_2^*, and the time interval between the images is Δt as follows:

$$\dot{\theta}^* = \frac{\theta_2^* - \theta_1^*}{\Delta t}. \tag{5}$$

Information regarding the fiber trajectory can be obtained from the flow visualization experiment. Sequential images of fibers traveling in an orifice channel can be image processed to extract the location, angle, and directional vector. However, the shear and extension rates of the flow must be calculated using a separate CFD simulation. The velocity field inside the orifice was calculated by modeling the identical channel configuration used in the flow visualization setup. The shear and extension rates from the CFD simulation were mapped to the fiber trajectory from image processing and subsequently used to calculate the theoretical angular velocity using Eq. (4).

A schematic illustration of the 2D model developed for the calculation of the shear and extension rates is shown in Fig. 3. It is identical to the cross section of the orifice channel used in the flow visualization experiment. The thicknesses of the narrow and expansion channels were 0.2 and 2 mm, respectively. The lengths of the narrow and expansion channels were 0.5 and 2 mm, respectively. An inlet velocity of 7.46 mm/s was applied to the left side of the narrow channel and the right side of the expansion channel was set as the pressure outlet boundary condition. The resulting Reynolds number (Re) in the expansion channel is set as 10^{-3}. The remaining walls were subjected to the no-slip boundary condition.

CFD calculations in the laminar flow regime were performed using ANSYS Fluent [32] based on finite-volume discretization. Double precision was utilized in this simulation to enhance the accuracy of the results. A second-order upwind scheme was selected for the discretization of the nonlinear mass and momentum equations to achieve a higher accuracy. The SIMPLE algorithm was adopted to couple the pressure and velocity. A convergence criterion of 10^{-6} was set for the continuity and momentum equations. A numerical simulation was performed to solve the following equations: [32]

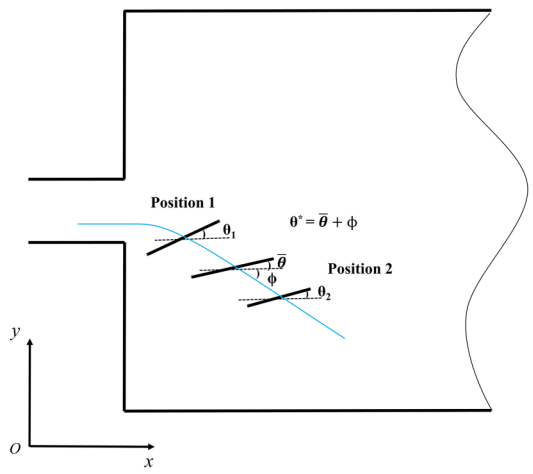

FIG. 2. Movement and rotation of a fiber along its trajectory inside the mold channel.

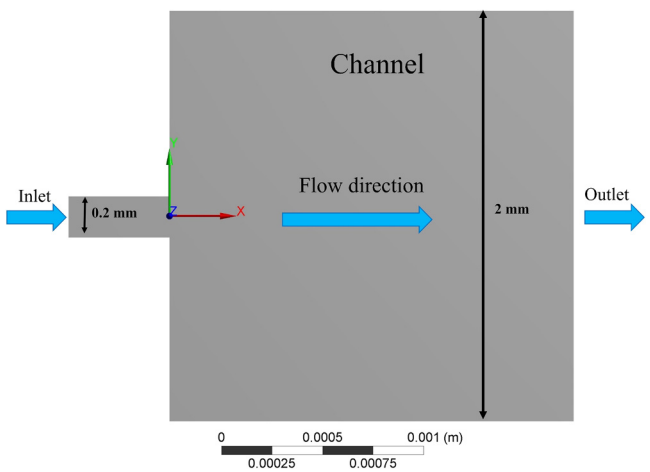

FIG. 3. Calculation domain of the mold channel for CFD simulation.

Continuity equation:

$$\nabla.(\rho \vec{u}) = 0. \tag{6}$$

Momentum equation:

$$\rho(\vec{u}.\nabla)\vec{u} = -\nabla p + \eta\nabla.(\nabla\vec{u} + \nabla\vec{u}^{T}), \tag{7}$$

where ρ, u, p, and η denote the density, velocity, pressure, and viscosity of the flow, respectively.

Uncured PDMS with a density of 1070 kg/m^3 was used as the working fluid. Because the viscosity and shear rate relationship of uncured PDMS exhibits a non-Newtonian behavior, the Carreau model was used to calculate the shear rate-dependent viscosity based on the following equation:

$$\eta = \eta_{\infty} + (\eta_0 - \eta_{\infty})\left[1 + \left(\lambda\dot{\gamma}\right)^2\right]^{\frac{n-1}{2}}, \tag{8}$$

where n, η_{∞}, η_0, and λ are the power-law index, infinite shear viscosity, zero shear viscosity, and time constant, respectively. The viscosity values of the PDMS and carbon mixture were obtained from a rotational rheometer at shear rates ranging from 0.1 to 2000 s^{-1}. Details regarding the measurements of the viscosity and shear rate are available in our previous paper [33].

A grid independence test was conducted using three different numbers of elements: 41 067, 256 240, and 456 060. The velocity profiles along the y-direction at $x = 0.1$ mm were compared among the three different element sizes. The deviation between cases involving the lowest and highest number of elements and intermediate and the highest number of elements were 6.433% and 0.105%, respectively. Therefore, the calculation result of the model with 456 060 elements was used to analyze the shear and extension rates.

III. EXPERIMENT APPARATUS

The experimental setup was identical to that used in our previous study [33]; the details are presented in Fig. 4. The experimental setup included three primary components: a high-speed camera, a mold channel, and a syringe pump, as shown in Fig. 4(a). The mold channel was fabricated using two Al blocks combined with two transparent acrylic windows, as shown in Fig. 4(b). The cross section of the mold channel was identical to that of the CFD model shown in Fig. 3. The width of the Al block was 20 mm. The front and back sides of the mold channel were shielded with two transparent acrylic plates as sealing and visualization windows. A plate-type LED lighting with a maximum power of 11 W was used to ensure sufficient brightness in the recorded images. A high-speed camera attached to a microscope with an objective lens of 2× magnification was used to capture consecutive images at a speed of 600 frames per second (fps). The fps of images analyzed for the fiber movement and rotation was reduced to 60 fps to save time and computational power. The resolution of the images was 1280 × 1024 pixels. The focal plane was adjusted to a distance of 1 mm from the transparent window.

A mixture of PDMS (Sylgard 184, Dow Corning Co., at a base to curing agent ratio of 10:1) and ball-milled carbon fiber (MFC, DowAksa Co) was used as the working fluid. The average length and diameter of the carbon fiber were 63 and 7 μm, respectively. The density of PDMS and carbon fiber are 965 and 1780 kg/m^3, respectively. No sedimentation of carbon fibers in the PDMS medium was observed during the experiment. The volume fraction of the carbon fiber in the suspension was fixed to 0.058%, and it was significantly

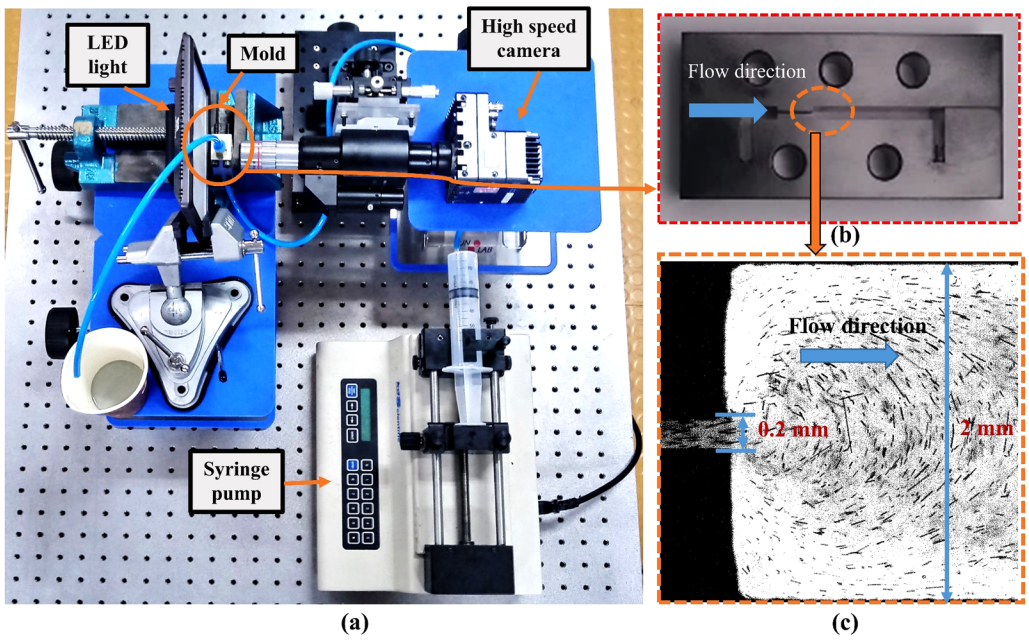

FIG. 4. Experiment apparatus for flow visualization. (a) Overall view of the experimental setup, (b) the mold channel, and (c) the image of PDMS and carbon fiber mixture inside the orifice channel.

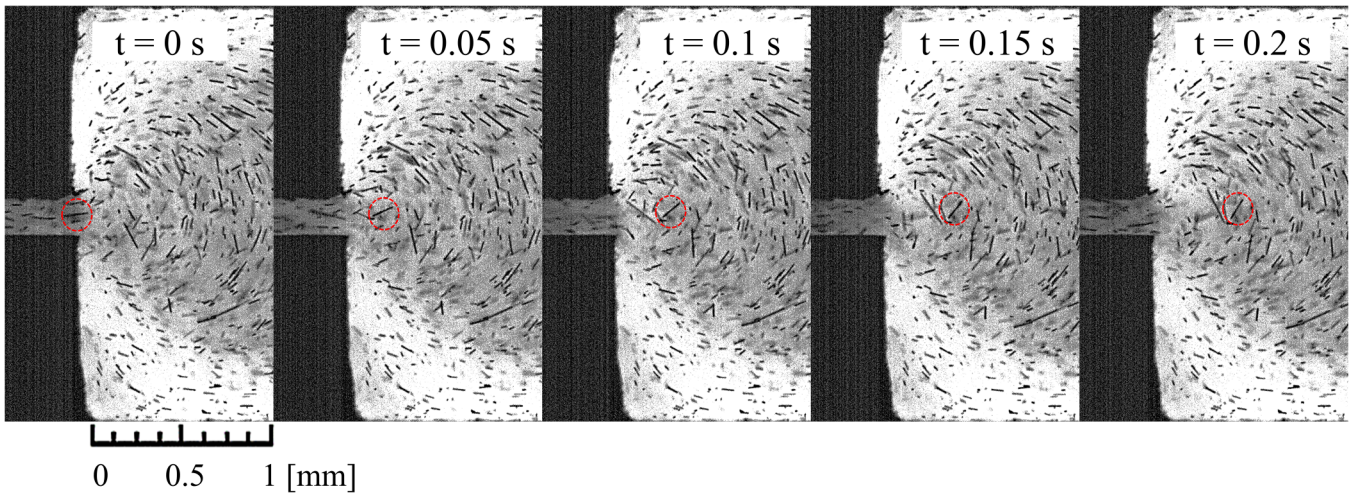

FIG. 5. Five consecutive flow visualization images showing a fiber (in dotted circle) traveling along the mold channel.

smaller than $1/AR^2 = 0.01235$, which represents a boundary value for the classification of dilute and semidilute suspensions [12]. Additionally, the product of the number density of the carbon fiber with the fiber average length was calculated to be 0.058, which also indicated a dilute suspension [34]. Therefore, interactions between fibers and the fiber-wall were neglected. Air bubbles capped inside the mixture were degassed at a vacuum pressure of ~50 Pa for 20 min. Subsequently, the PDMS and carbon fiber mixture were stored inside a 50 ml syringe and placed on a syringe pump (KDS410, KD Scientific). The pumping speed was fixed based on the Re number (10^{-3}) inside the expansion channel.

The location, alignment angle, and length of fibers in the flow visualization images were obtained via image processing. First, the brightness and contrast of the images captured by the high-speed camera were adjusted to distinguish the fibers on the focal plane. The brightness of the unfocused fibers and the background were controlled to similar values, whereas the pixels that compose the focused fibers were recognized. Subsequently, the pixels on the image were scanned to trace the pixels of the fibers along with the connecting structure of the fiber to calculate the end locations. The end locations of the fibers were used to calculate the center location, length, and alignment angle. After all the fibers in the image were scanned and analyzed, consecutive flow visualization images were processed. The fiber was manually monitored in the consecutive images, and the location and angle change of the fiber were analyzed as shown in Fig. 5. More details regarding the image processing method are available in the literature [20].

As shown in Fig. 5, a fiber (inside the dotted circle) was selected and monitored after it exited from the narrow channel. The time of $t = 0$ s is defined as the start of the sampling time. At 0.2 s, the fiber has traveled 0.45 mm and an angle change of 50° can be noticed. Information regarding the fiber velocity, alignment angle, trajectory path, etc., was further analyzed from the recorded coordination of the fiber. Approximately 20 fibers were analyzed per flow visualization image. To understand the rotation and movement of a fiber, the shear and extension rates along the fiber trajectory were calculated from CFD simulation. The comparison between the experiment and CFD results are presented in Sec. IV.

IV. RESULT AND DISCUSSION

Because the CFD modeling and boundary conditions were set based on the experimental conditions of the flow visualization, we can correlate the shear and extension rates to the rotation of a fiber inside the mold channel. The shear and extension rates calculated via CFD simulation are shown in Fig. 6. The shear rates shown in Fig. 6(a) exhibited symmetrical values with opposite signs at the narrow and expansion channels in the direction of the channel thickness. This is because the coordinate axis was located at the center of the outlet of the narrow channel (shown in Fig. 3). Therefore, the shear rate distribution ($\partial u/\partial y$) has negative and positive values at the top half and bottom half regions of the channel, respectively. In the expansion channel, the absolute value of the shear rate decreased rapidly to less than 1/10 of the value inside the narrow channel. This is because the flow cross section increased by 10 times compared with those of the narrow channels. At the exit of the narrow channel, the flow velocity decreased to ~1/10, and the flow directions spread radially to the top, center, and bottom of the expansion channel. Owing to this spreading, the extension rate changed abruptly at the exit of the narrow channel and at the entry of the expansion channel, as shown in Fig. 6(b).

Based on the positions of fibers from the experimental result, the shear and extension rates along the fiber trajectories were obtained from the CFD calculation. To validate the results obtained using the image processing, 70 fibers were illustrated as arbitrary lines with known locations, lengths, and angles. Subsequently, the location, length, and angles yielded by the image processing were compared with the actual values. A maximum error of ~3° was observed for the fiber angles obtained from the image processing procedure. To consider the motion of the fibers along its path, five representative fibers traveling in different regions of the mold channel were monitored as shown in Fig. 7. These fibers were selected to represent the top, middle, and bottom

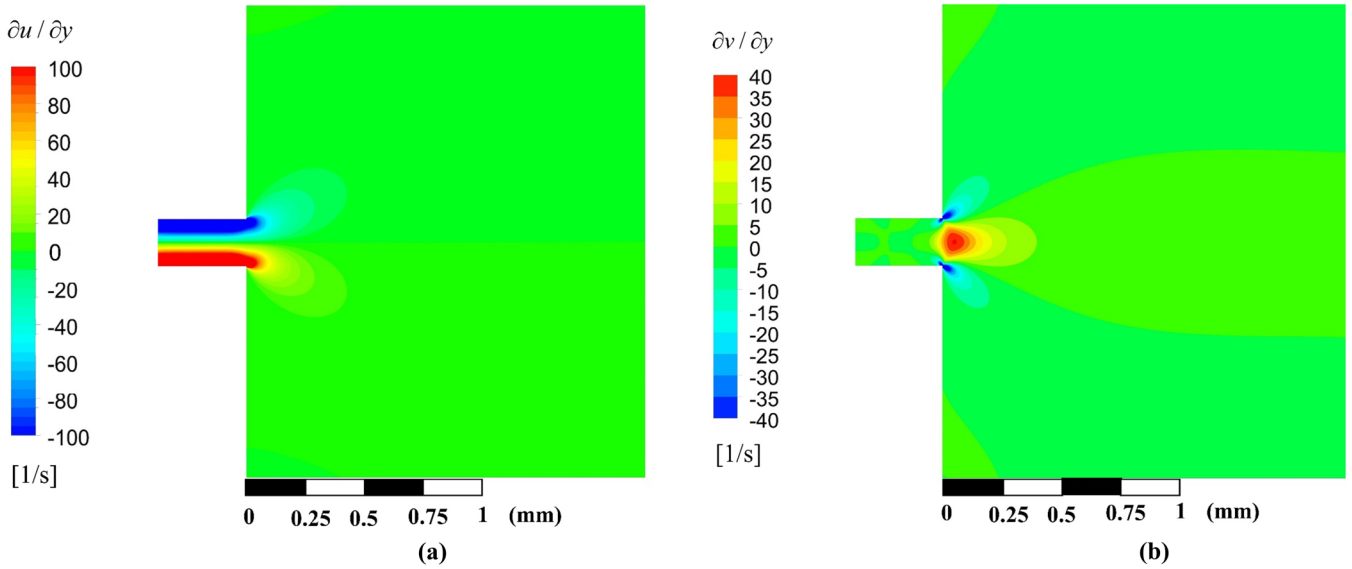

FIG. 6. CFD calculation results of (a) the shear rate and (b) the extension rate in the mold channel (Re = 0.001).

regions inside the expansion channel. The movement and rotation of each fiber were reconstructed, as shown in Fig. 7(a). The time interval between consecutive movements were set as an arbitrary value since the velocities of fibers were different.

Fibers 1 and 2 ascended to the top of the channel, fiber 3 propagated at the center of the channel, and fibers 4 and 5 descended from the channel. The fibers that passed out of the corners of the orifice walls indicated angle changes that were more significant than those passed at the center region. Owing to the flow velocity gradient in the y-direction, the fibers passed through the top and bottom corners of the outlet of the narrow channel in counter-clockwise and clockwise movements, respectively. In contrast, the fiber that traveled at the center region of the channel indicated slight angle changes, and those fibers propagated perpendicular to the fluid flow downstream within the channel. A numerical simulation was performed to obtain the shear and extension rates for every fiber, as shown in Fig. 7(b). By monitoring the fiber positions, the fiber locations were identified, and then the shear and extension rates were specified at those positions. The shear rate was found to be much larger than the extension rate. The magnitude of the shear and extension rates changed significantly from position $x = 0$ to 0.2 mm. Subsequently, both the shear and extension rates remained almost unchanged from $x = 0.2$ to 0.5 mm. Based on the reconstructed fiber, it was discovered that the movement of fibers 1 and 5 from the corners of orifice to location

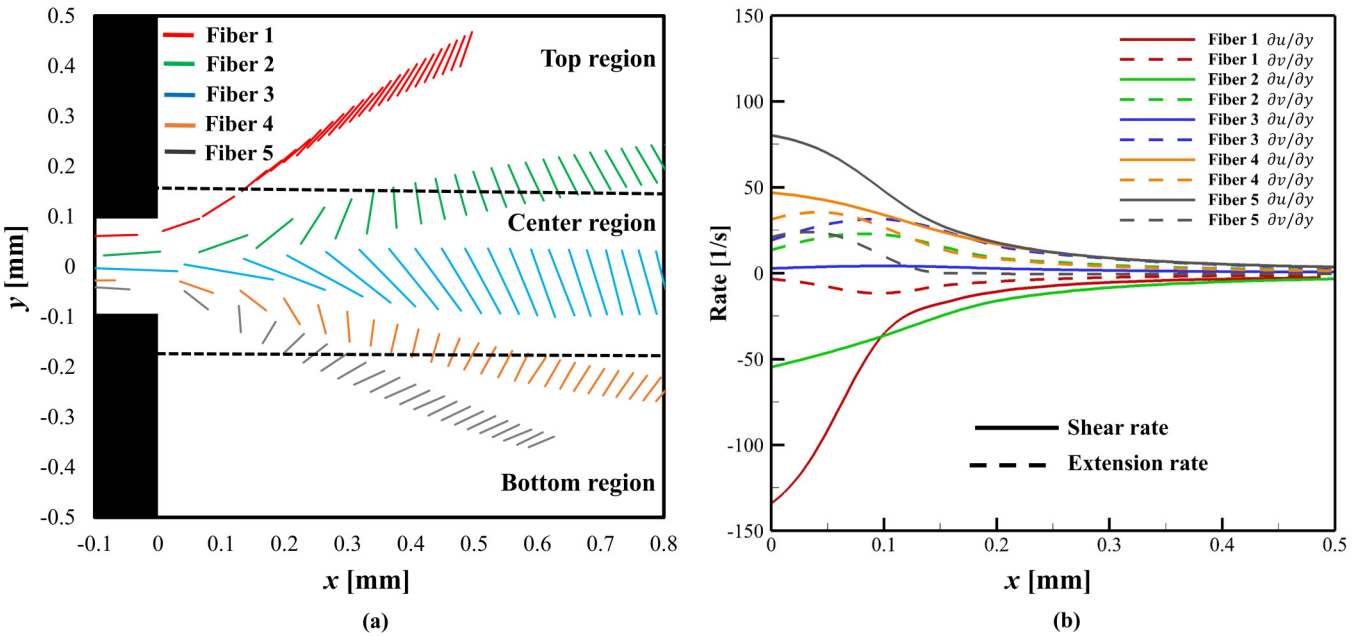

FIG. 7. Carbon fiber monitoring in the orifice channel (Re = 0.001). (a) Movement and rotation of five representative fibers from the flow visualization experiment; (b) shear and extension rates on five fibers.

$x \sim 0.2$ mm yielded the highest shear rate compared with other fibers. This phenomenon was consistent with the expectation that the effect of shear rate induces a rapid change in the fiber angle near the orifice corners and a slow change in angle downstream of the channel.

To check the dependency of the flow visualization results with different frame rates, velocity, angular velocity, and shear and extension rates of fiber 2 were calculated in 30, 60, and 150 fps and presented in Fig. 8. The velocities, angular velocity, and shear and extension rates along the fiber trajectory are shown in Figs. 8(a)–8(c), and a good agreement between different frame rate results can be noticed. Although the uncertainties in approximation error of linearization and error in coordinate location resulted in the scattering of the velocity and angular velocity results in the vicinity of the narrow channel outlet was observed, no sign of dependence on the frame rates was found. To ensure accurate and efficient image processing of flow visualization images, a frame rate of 60 fps was selected in the present study.

The results of the present study were compared with Jeffery's theory [5]. The angular velocity of carbon fibers as a function of the fiber angle and the effective shear rate is shown in Fig. 9. When comparing the effective shear rate of a fiber, the x and y coordinates of the fiber are calculated from a flow visualization image. Then the shear and extension rates of the corresponding coordinate are mapped from the CFD result and assigned to each fiber along the movement trajectories. Since there is a limited number of fibers from the experiments, the angular velocity values in the experimental data shown in Fig. 9(a) were selected to have a deviation of ±10% of the effective shear rate. For example, data of fibers at the effective shear rate of 5 s^{-1} are chosen from the fibers that show effective shear rate ranging from 4.5 to 5.5 s^{-1}. A similar deviation of ±10% of angle was applied to when classifying angular velocity of fibers at various angles as shown in Fig. 9(b).

According to Jeffery's theory, as illustrated in Fig. 9(a), the maximum angular velocity was recorded at angles of −90° and 90°, whereas the minimum value was recorded at 0°. In addition, the angular velocity increased as the effective shear rate increased from 5 to 20 s^{-1}. However, effect of AR to the angular velocity can be neglected; for example, comparing difference in angular velocity when AR is changed from 6 to 12 shows only 2.02% deviation. The experimental angular velocities show a somewhat constant value depending on the effective shear rate, unlike Jeffery's equation. The negligible difference in experimental angular velocity can be noticed with changes in the fiber angle and AR.

The difference between the experimental result and Jefferey's theory can be attributed to the abrupt change of velocity field at the vicinity of the outlet of the narrow channel. At the outlet of the narrow channel, a sudden decrease in u and rapid rise and fall of v can be inferred from the distribution of the shear and extension rates as shown in Fig. 6. The length scale of these sudden change of velocity components is less than 100 μm and is comparable to the length of a fiber. Although the changes in the flow direction were accounted in Eqs. (2) and (3) for the calculation of the fiber angle and the effective shear rate, the overall shear rate on a fiber needs to be integrated along the fiber length in such a complex flow field. Instead, we indicated the shear and extension rates of the center location of fiber to represent the overall effective shear rate on the fiber. This assumption may result in the difference between the experimental results and Jeffery's theory. However, it is not clear why the angular velocity obtained by the experiment shows negligible deviation with the change in the fiber angle. It will be further researched by the detailed analysis on the distribution of shear and extension rates along with the fiber from a larger number of sampling fibers in the future study.

The angular velocity increased with both the shear and extension rates. It is noteworthy that the high shear and extension rates were observed at the outlet of the narrow channel, whereas low values were observed along the downstream of the expansion channel. In the present study, the magnitudes of the shear and extension rates at the outlet of the narrow channel were approximately 130 and 45 s^{-1}, respectively. Subsequently, they decreased along the downstream flow direction, implying that the effects of shear and extension rates at that position did not induce the rotation of the additive; therefore, the carbon fibers exhibited only translational motion. As shown in Figs. 9(a) and 9(b), the angular velocity of the experimental data is observed to depend only on the effective shear rate. Therefore, the angular velocity was expressed as a function of the shear and extension rates based on the studies of Tu and Phu [35,36]. An expression for the angular velocity of the carbon fiber as a function of

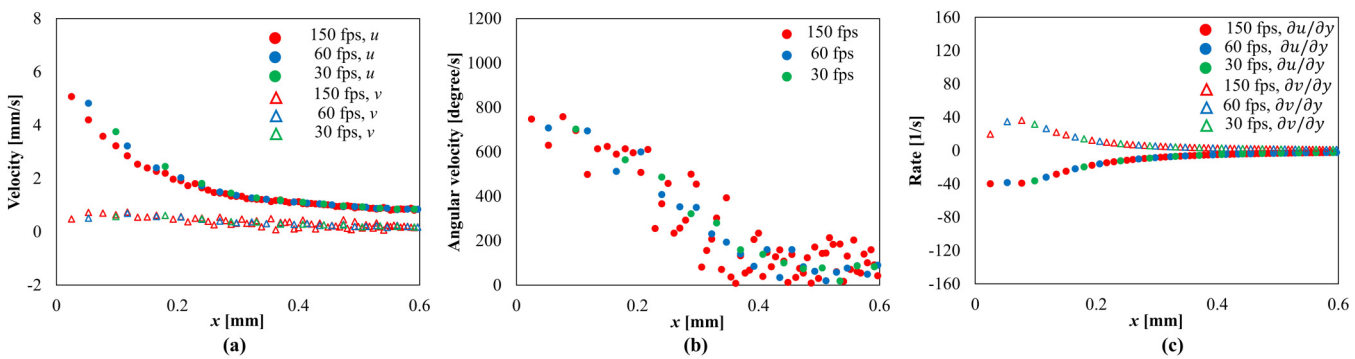

FIG. 8. Flow visualization result of fiber 2 in different frame rates of 30, 60, and 150 fps showing (a) u and v; (b) angular velocity; and (c) shear and extension rates.

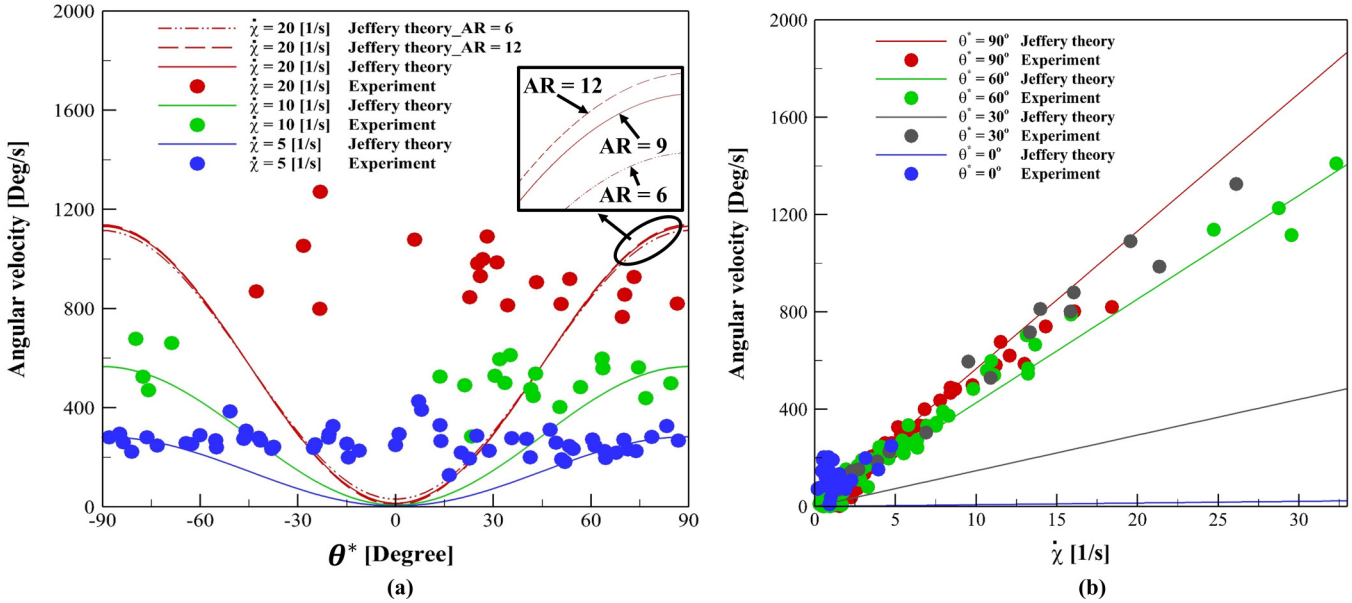

FIG. 9. Angular velocity as a function of (a) the fiber angle and (b) the effective shear rate between the present study and Jeffery's theory.

the shear and extension rates was established as follows:

$$\dot{\theta} = 51.17 \times \sqrt{\frac{1}{2}\left|\frac{\partial u}{\partial y} \times \frac{\partial v}{\partial y}\right|}. \tag{9}$$

The predicted correlation function was compared with the experimental data that are plotted and shown in Fig. 10.

To observe the agreement between the correlation function and the experimental data, the multiplanes of the shear and extension rates are shown in Fig. 11. Because the experimental results of shear and extension rates did not match exactly to denoted rates, data within a deviation of ±10% are included to represent the experimental values in Fig. 11. The angular velocity as a function of shear rate at three typical planes with extension rates of 5, 10, and 15 s^{-1} is shown in Fig. 11(a). The angular velocity of the carbon fibers increased with the shear rate. The results indicated a good agreement between the prediction and experimental data. Similarly, the angular velocity as a function of the extension rate at three typical planes with shear rates of 10, 30, and 50 s^{-1} is shown in Fig. 11(b). The angular velocity of the carbon fibers increased with the extension rate. The results indicate consistency between the prediction and experimental data. The maximum error between the experimental data and prediction results was 12%.

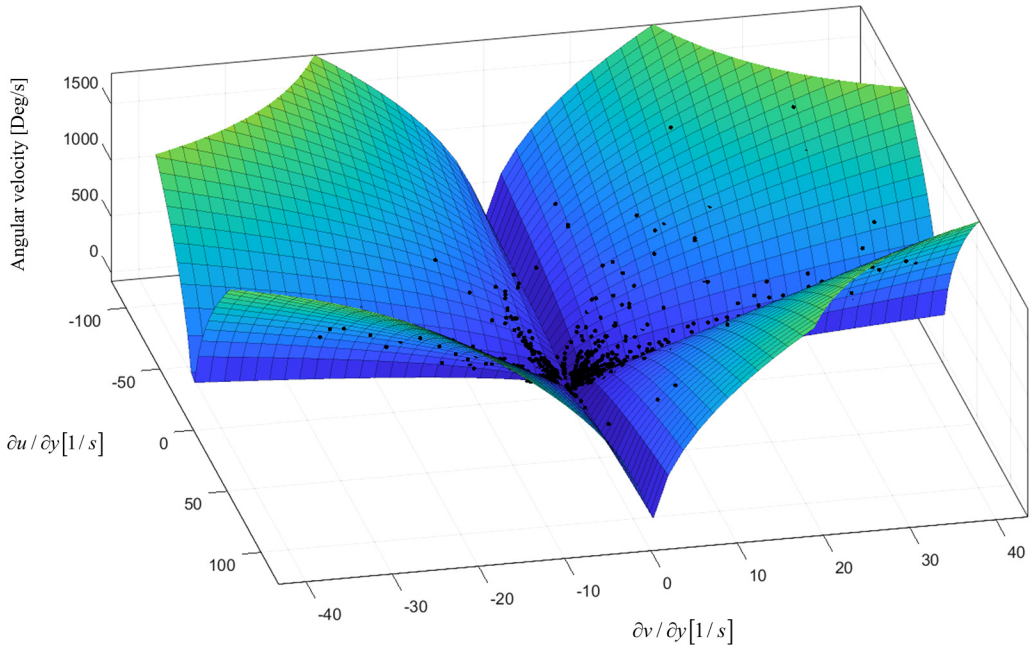

FIG. 10. Correlation function of angular velocity as functions of shear and extension rates.

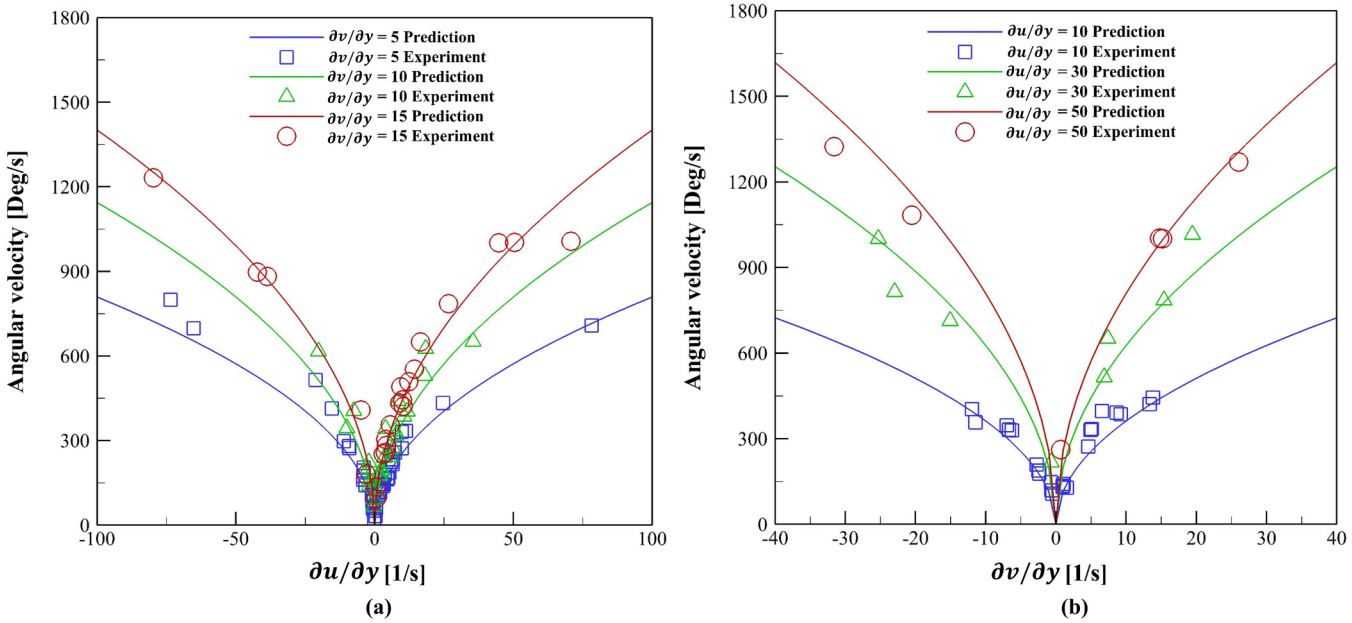

FIG. 11. Angular velocity between the experiment and prediction. Multiplanes of (a) the extension rate and (b) the shear rate.

The prediction and experimental data of angular velocities inside the channel for five typical fibers along the flow direction are shown in Fig. 12. The results show that the high angular velocity of the carbon fibers occurred at position $x \sim 0.05$ mm for all five typical fibers. Subsequently, it decreased rapidly along the flow from position $x = 0.05$ to 0.2 mm, followed by a gentle decrease from position $x = 0.2$ to 0.6 mm. Finally, from position $x = 0.6$ mm to the downward stream, the angular velocity remained unchanged in the channel, and the carbon fibers exhibited only translational motion without rotation. Fibers 1 and 2 ascended to the top of the channel, fiber 3 propagated at the center of the channel, and fibers 4 and 5 descended from the channel. Among the five typical fibers, the fibers traveling near to the walls of the expansion channel showed highest angular velocity compared to the fiber traveling in the center region. This is because the high shear and extension rates at the corners of the narrow channel outlet induced a high angular velocity in the carbon fibers. Subsequently, the shear and extension rates decreased along the downstream of the channel, resulting in a decreased angular velocity in the fiber. The highest deviation between the prediction and experimental data was recorded at position $x \sim 0.05$ mm, i.e., 16.67%. This may be because the fibers are located at positions that are far from the dominant region of the strong extension rate as shown in Fig. 6(b). Additionally, at $x < 0.05$ mm, changes in shear and extension rates were abrupt and nonlinear to be fitted in a simple linear correlation. Nevertheless, the prediction and experimental data of angular velocities inside the orifice channel indicated good agreement. For a better visualization, the angular velocity contours along the orifice channel based on the prediction and experiment are shown in Fig. 13.

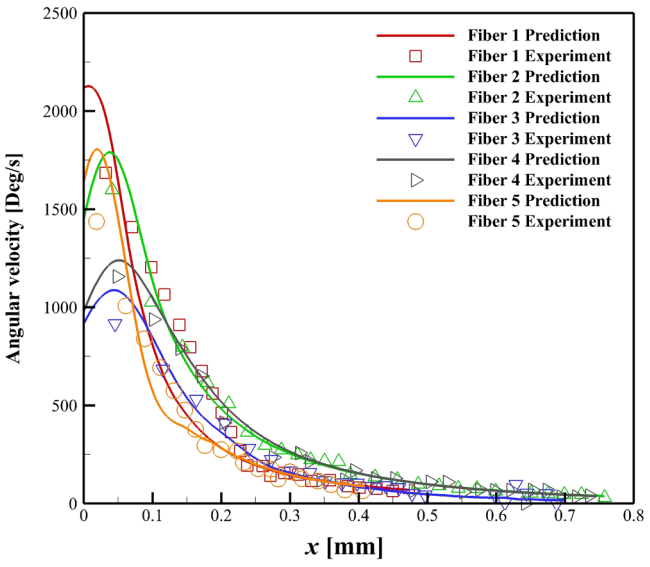

FIG. 12. Angular velocities of five typical fibers along the flow direction obtained from simulation and the experiment.

The angular velocity contours obtained from the simulation and experiment are shown in Fig. 13. The results from the correlation function agreed well with the experimental data. As shown from the simulation results, high angular velocities of the carbon fiber were recorded in the upper and lower corner regions of the outlet of the narrow channel. The highest angular velocity appeared primarily at position $x = 0.05$ mm with a magnitude of 1800 °/s. Subsequently, the angular velocity reduced at position $x = 0.2$ mm to a magnitude of approximately 500 °/s. Finally, the angular velocity remained constant along the downstream of the expansion channel. This shows that the carbon fiber motion under a low effective shear rate results in only a translational motion without rotation.

By applying this correlation function, the angular velocity within the expansion channel was specified. This approach can be utilized in other parts of the mold channel to predict

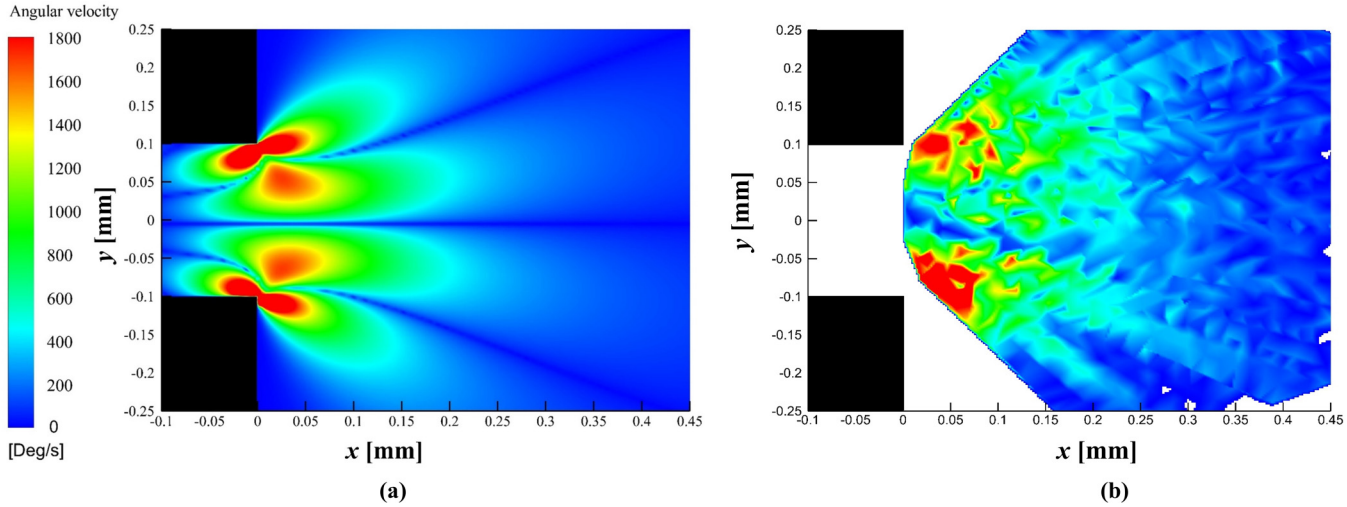

FIG. 13. Angular velocity contour between simulation and the experiment: (a) Simulation results from correlation and (b) results from the experiment.

the angular velocity of the additive and resulting orientation distribution for the analysis of the anisotropic physical property of the final products. Further research is required to expand the proposed method to be applied to account for higher concentration and different types of additive, a wider range of channel configuration, and various conditions in the injection molding process. Nevertheless, we believe that the proposed method is more simple and straightforward and requires less computational power to calculate the alignment angle of additives in comparison to conventional models and methods. Additionally, our approach should enhance the understanding of additive alignment during the molding process and also be used to validate and enhance the accuracy of conventional models.

V. CONCLUSION

Experiments and numerical simulations were performed to investigate the additive behavior inside a mixture of carbon fibers and PDMS flowing in an orifice channel during the injection molding of polymer composites. The numerical simulation of the identical orifice channel was performed and calculation result of the flow field was compared to the experimental result. The fiber angle, extension rate, and shear rate along the additive path in the channel were monitored to analyze the angular velocity of the carbon fiber during injection molding. A functional relationships of angular velocity in terms of the shear rate and the extension rate were established, with a maximum error of 12% between the experimental data and prediction results.

A correlation to predict the angular velocity of the carbon fibers along the flow direction within the channel was presented and validated using experimental data. The prediction and experimental results of angular velocity indicated good agreement in terms of the additive behavior within the channel. The carbon fiber indicated high angular velocities at the top and bottom corners of the outlet of the narrow channel. Subsequently, the magnitudes decreased along the downward fluid flow inside the channel. By applying the correlation function of the angular velocity, the angular velocity within the channel can be specified; consequently, the additive alignment in an orifice channel during the injection molding of polymer composites can be determined.

ACKNOWLEDGMENTS

This study was supported by the Basic Science Research Program through the National Research Foundation of Korea (NRF) funded by the Ministry of Education (No. NRF-2019R1I1A3A01061335).

NOMENCLATURE

AR	Aspect ratio
n	Power-law index
p	Pressure (Pa)
Re	Reynolds number
u	Velocity (m/s)
x, y	Cartesian coordinate system

Subscripts

2	Second position
1	First position
0	Zero
∞	Infinity
$\dot{\gamma}$	Shear rate (1/s)
$\dot{\varepsilon}$	Extension rate (1/s)
η	Viscosity (Pa s)
$\dot{\theta}$	Angular velocity (°/s)
$\dot{\chi}$	Effective shear rate (1/s)
ρ	Density (kg/m^3)

REFERENCES

[1] Wang, M., Q. Kang, and N. Pan, "Thermal conductivity enhancement of carbon fiber composites," Appl. Therm. Eng. **29**, 418–421 (2009).

[2] Fu, S. Y., and Y. W. Mai, "Thermal conductivity of misaligned short-fiber-reinforced polymer composites," J. Appl. Polym. Sci. **88**, 1497–1505 (2003).

[3] Gupta, M., and K. Wang, "Fiber orientation and mechanical properties of short-fiber-reinforced injection-molded composites: Simulated and experimental results," Polym. Compos. **14**, 367–382 (1993).
[4] Nguyen, B. N., S. K. Bapanapalli, J. D. Holbery, M. T. Smith, V. Kunc, B. J. Frame, J. H. Phelps, and C. L. Tucker III, "Fiber length and orientation in long-fiber injection-molded thermoplastics—Part I: Modeling of microstructure and elastic properties," J. Compos. Mater. **42**, 1003–1029 (2008).
[5] Jeffery, G. B., "The motion of ellipsoidal particles immersed in a viscous fluid," Proc. R. Soc. London A **102**, 161–179 (1922).
[6] Taylor, G. I., "The motion of ellipsoidal particles in a viscous fluid," Proc. R. Soc. London A **103**, 58–61 (1923).
[7] Trevelyan, B., and S. Mason, "Particle motions in sheared suspensions. I. Rotations," J. Colloid Sci. **6**, 354–367 (1951).
[8] Altan, M., S. Advani, S. Güçeri, and R. Pipes, "On the description of the orientation state for fiber suspensions in homogeneous flows," J. Rheol. **33**, 1129–1155 (1989).
[9] Batchelor, G., "Slender-body theory for particles of arbitrary cross-section in stokes flow," J. Fluid Mech. **44**, 419–440 (1970).
[10] Bretherton, F. P., "The motion of rigid particles in a shear flow at low reynolds number," J. Fluid Mech. **14**, 284–304 (1962).
[11] Krochak, P., J. Olson, and D. Martinez, "Near-wall estimates of the concentration and orientation distribution of a semi-dilute rigid fibre suspension in poiseuille flow," J. Fluid Mech. **653**, 431–462 (2010).
[12] Papathanasiou, T., and D. C. Guell, *Flow-Induced Alignment in Composite Materials* (Woodhead, Abington, England, 1997).
[13] Sierra-Romero, A., and B. Chen, "Strategies for the preparation of polymer composites with complex alignment of the dispersed phase," Nanocomposites **4**, 137–155 (2018).
[14] Siqueira, I., R. Rebouças, and M. Carvalho, "Migration and alignment in the flow of elongated particle suspensions through a converging-diverging channel," J. Non-Newtonian Fluid Mech. **243**, 56–63 (2017).
[15] Zhang, L.-Z., X.-J. Wang, Y.-Y. Quan, and L.-X. Pei, "Conjugate heat conduction in filled composite materials considering interactions between the filler and base materials," Int. J. Heat Mass Transfer **64**, 735–742 (2013).
[16] Zhou, B., W. Luo, J. Yang, X. Duan, Y. Wen, H. Zhou, R. Chen, and B. Shan, "Simulation of dispersion and alignment of carbon nanotubes in polymer flow using dissipative particle dynamics," Comput. Mater. Sci. **126**, 35–42 (2017).
[17] Wittemann, F., R. Maertens, L. Kärger, and F. Henning, "Injection molding simulation of short fiber reinforced thermosets with anisotropic and non-Newtonian flow behavior," Compos. A: Appl. Sci. Manuf. **124**, 105476 (2019).
[18] Chiba, K., S. Hayashi, K. Kojima, K.-W. Song, K. Nakamura, and A. Horikawa, "Fiber orientation in fiber suspension flow through a parallel plate channel and an abrupt contraction channel," J. Text. Mach. Soc. Jpn. **37**, 67–72 (1991).
[19] Stasiak, J., J. Brubert, M. Serrani, S. Nair, F. de Gaetano, M. L. Costantino, and G. D. Moggridge, "A bio-inspired microstructure induced by slow injection moulding of cylindrical block copolymers," Soft Matter **10**, 6077–6086 (2014).
[20] Park, J. Y., and D.-W. Oh, "Image processing of additive alignment inside a polydimethylsiloxane and carbon fiber mixture flow," J. Mech. Sci. Technol. **33**, 2203–2209 (2019).
[21] Shaharuddin, S. I. S., M. Salit, and E. S. Zainudin, "A review of the effect of moulding parameters on the performance of polymeric composite injection moulding," Turk. J. Eng. Environ. Sci. **30**, 23–34 (2006).
[22] Parandoush, P., and D. Lin, "A review on additive manufacturing of polymer-fiber composites," Compos. Struct. **182**, 36–53 (2017).
[23] Oumer, A. N., and O. Mamat, "A review of effects of molding methods, mold thickness and other processing parameters on fiber orientation in polymer composites," Asian J. Sci. Res. **6**, 401–410 (2013).
[24] Trebbin, M., D. Steinhauser, J. Perlich, A. Buffet, S. V. Roth, W. Zimmermann, J. Thiele, and S. Förster, "Anisotropic particles align perpendicular to the flow direction in narrow microchannels," Proc. Natl. Acad. Sci. U.S.A. **110**, 6706–6711 (2013).
[25] Folgar, F., and C. L. Tucker, "Orientation behavior of fibers in concentrated suspensions," J. Reinf. Plast. Compos. **3**, 98–119 (1984).
[26] Advani, S. G., and C. L. Tucker, "The use of tensors to describe and predict fiber orientation in short fiber composites," J. Rheol. **31**, 751–784 (1987).
[27] Meyer, K. J., J. T. Hofmann, and D. G. Baird, "Prediction of short glass fiber orientation in the filling of an end-gated plaque," Compos. A: Appl. Sci. Manuf. **62**, 77–86 (2014).
[28] Meyer, K. J., J. T. Hofmann, and D. G. Baird, "Initial conditions for simulating glass fiber orientation in the filling of center-gated disks," Compos. A: Appl. Sci. Manuf. **49**, 192–202 (2013).
[29] VerWeyst, B. E., and C. L. Tucker, "Fiber suspensions in complex geometries: Flow/orientation coupling," Can. J. Chem. Eng. **80**, 1093–1106 (2002).
[30] Baloch, A., and M. F. Webster, "A computer simulation of complex flows of fibre suspensions," Comput. Fluids **24**, 135–151 (1995).
[31] Bird, R. B., W. E. Stewart, and E. N. Lightfoot, *Transport Phenomena* (John Wiley & Sons, New York, 1960), p. 413.
[32] Fluent, A., *17.0 Theory Guide* (ANSYS, Inc., Canonsburg, PA, 2015), 15317.
[33] Nguyen, H. M. K., and D.-W. Oh, "Analysis of carbon fiber alignment in a polydimethylsiloxane matrix flowing in an orifice channel," J. Mol. Liq. **317**, 113978 (2020).
[34] Doi, M., and S. F. Edwards, *The Theory of Polymer Dynamics* (Clarendon, Oxford, 1986).
[35] Ngo, T. T., and N. M. Phu, "Computational fluid dynamics analysis of the heat transfer and pressure drop of solar air heater with conic-curve profile ribs," J. Therm. Anal. Calorim. **139**, 3235–3246 (2020).
[36] Phu, N. M., V. Tuyen, and T. T. Ngo, "Augmented heat transfer and friction investigations in solar air heater artificially roughened with metal shavings," J. Mech. Sci. Tech. **33**, 3521–3529 (2019).